# Crystal structure, Hirshfeld surface analysis, quantum mechanical study and spectroscopic studies of noncentrosymmetric (S)nicotiniumtrichloridozincate monohydrate complex

S Soudani, V Ferretti, C Jelsch, F Lefebvre, C Ben Nasr

**Published in Inorganic Chemistry Communications**
Volume 61, November 2015, Pages 187-192

doi.org/10.1016/j.inoche.2015.09.021

# Crystal Structure, Hirshfeld Surface Analysis, Quantum Mechanical Study and Spectroscopic Studies of Non-centrosymmetric (S)nicotinium-trichloridozincate Monohydrate Complex

S. Soudani[a], V. Ferretti[b], C. Jelsch[c], F. Lefebvre[d], C. Ben Nasr[a]

[a]Université de Carthage, Laboratoire de Chimie des Matériaux, Faculté des Sciences de Bizerte, 7021 Zarzouna, Tunisie.

[b]Department of Chemical and Pharmaceutical Sciences and Center for Structural Diffractometry, via Fossato di Mortara 17, I-44121 Ferrara, Italy.

[c]CRM2, CNRS, Institut Jean Barriol, Université de Lorraine, Vandoeuvre les Nancy CEDEX, France.

[d]Laboratoire de Chimie Organométallique de Surface (LCOMS), Ecole Supérieure de Chimie Physique Electronique, 69626Villeurbanne Cedex, France.

Corresponding e-mail: cherif_bennasr@yahoo.fr

## Abstract

The chemical preparation, crystal structure and spectroscopic characterization of the novel noncentrosymmetric (S)-nicotiniumtrichloridozincate monohydrate complex have been reported. The atomic arrangement can be described as built up by chains of $ZnNCl_3$ tetrahedra and water molecules, interconnected via O-H…Cl hydrogen bonds. The organic entities are inserted between these chains through C-H…Cl and N-H…Cl hydrogen bonds. The 3D

Hirshfeld surfaces and the associated 2D fingerprint plots were investigated for intermolecular interactions. The $^{13}C$ and $^{15}N$ CP-MAS NMR spectra are in agreement with the X-ray structure. The vibrational absorption bands were identified by infrared spectroscopy. DFT calculations allowed the attribution of the NMR peaks.

**Keywords:** Trichloridozincate; X-ray diffraction; intermolecular contacts; quantum calculations; NMR; DFT calculations

## Introduction

Transition metal complexes play a very important role in many areas of chemistry and biology, such as catalysis [1,2], medicinal chemistry [3], photochemistry and electrochemistry [4] and so on. Zn(II) complexes, in particular, are related to almost all these research areas being used, for instance, as antidiabetic metallo pharmaceutic compounds [5], as catalysts in asymmetric Michael additions [6] or as photoluminescent molecules [7]. In general, transition metal complexes are very versatile compounds, being able to assume a variety of molecular geometries, such as tetrahedral, square planar, square pyramidal, trigonal bipyramidal and octahedral [8], and to modulate their properties by changing the organic ligands. In the crystalline state, for example, the crystal packing is often established on the base of the non-covalent interactions occurring between the organic ligands, e.g. hydrogen bonds or π-π stacking. It is worthy to note that these same weak forces play a vital role in molecular recognition, self-organization of molecule and highly efficient and specific biological reactions associated with supramolecular chemistry [9]. As for the organic ligand, we focused our attention on nicotine, a molecule extracted from the Nicotiana tabacum plant, although it is found in smaller amounts amongst other plants of the Solanaceae family. It is an interesting molecule with different applications, since it displays beneficial effects on patients suffering from Parkinson's disease, anxiety, schizophrenia, Alzheimer's disease, ulcerative colitis, and other CNS disorders [10–13]. Previous work on the coordination chemistry of nicotine has been

limited to a few studies, and only a restricted number of crystal structures of complexes have been described.

As a part of our continued involvement in the investigation of metal halide complexes of nitrogen containing ligands, we report here the synthesis, structure determination, investigation of intercontacts by Hirshfeld surface analysis and spectroscopic studies of a new non-centrosymmetric nicotinium trichloridozincate complex.

## Experimental

*Chemical preparation*

A solution of (S)-3-(1-methyl-2-pyrrolidinyl)pyridine (0.16 g, 1 mmol; Aldrich, purity ≥99% (GC)) dissolved in 15 mL absolute ethanol and $ZnCl_2$ (0.13 g, 1 mmol; Aldrich, purity 98%) dissolved in water, were mixed with an aqueous HCl solution (2 M, 20 mL). The resulting solution was evaporated slowly at room temperature over a period of several days, leading to the formation of transparent colorless prismatic crystals with suitable dimensions for single crystal structural analysis. The crystals were isolated after several days and subjected to X-ray diffraction analysis. They are stable for months under normal conditions of temperature and humidity (yield 73%). Analysis. Calc.: C, 33.99%; H, 28.31; N, 7.93 %. Found: C, 33.84; H, 28.47; N, 7.99%.

*Investigation techniques*

The characterization of the investigated compounds was performed using X-ray diffraction, solid-state NMR and IR spectroscopy techniques.

*X-ray single crystal structural analysis*

A single crystal was carefully selected under polarizing microscope in order to perform its structural analysis by X-ray diffraction. Diffraction data were collected on a Nonius Kappa

diffractometer equipped with a CCD detector with graphite-monochromatized MoKα radiation (λ=0.71069Å). Intensities were corrected for Lorentz polarization and absorption effects [14]. The structure was solved by direct methods with the SIR97 suite of programs [15] and refinements were performed on $F^2$ by full-matrix least-squares methods with all non-hydrogen atoms anisotropic. Hydrogens bound to C atoms were included at calculated positions, riding on their carrier atoms; the N-H hydrogen atom was found in the difference Fourier map. All hydrogen atoms were refined isotropically. All calculations were performed using SHELXL-2014 [16] implemented in the WINGX system of programs [17]. The crystal data are reported in Table 1. The drawings were made with Diamond [18] and Mercury [19]. Hirshfeld surface analyses were carried out and finger print plots were plotted using CrystalExplorer [20]. Electrostatic potentials were calculated using Avogadro 1.0.0[21].

*NMR and IR measurements*

The NMR spectra were recorded on a solid-state high-resolution Bruker DSX-300 spectrometer operating at 75.49 MHz for $^{13}C$ and 30.30 MHz for $^{15}N$ with a classical 4 mm probe head allowing spinning rates up to 10 kHz. $^{13}C$ and $^{15}N$ NMR chemical shifts are given relative to tetramethylsilane and neat nitromethane, respectively (precision 0.5 ppm). The spectra were recorded by use of cross polarization (CP) from protons (contact time 5 ms) and magic angle spinning (MAS). Before recording the spectrum it was checked that there was a sufficient delay between the scans allowing a full relaxation of the protons. The IR spectra were recorded in the range 4000–400 $cm^{-1}$ with a ‘‘Perkin–Elmer FTIR’’ spectrophotometer1000 using samples dispersed in spectroscopically pure KBr pressed into a pellet.

The NMR chemical shifts were calculated with the Gaussian 09 software. All calculations were made at the B3LYP/6-311++G** level. The positions of the atoms were those determined by the X-ray diffraction study except for the hydrogen atoms which were first

optimized at the same level of theory. Indeed the positions determined by X-ray do not correspond to the location of the proton but to that of the barycenter of the electron density. The chemical shifts were then calculated by use of the GIAO method.

## Results and discussion

*Structure description*

The asymmetric unit of the title compound contains one protonated nicotine amine ligand ((2S)-1-methyl-2-pyridin-3-yl-pyrrolidinium) coordinating to a zinc atom, that is further bonded by three chlorine atoms in a slightly distorted tetrahedral geometry, and a water molecule (Fig. 1). The whole complex has a zwitterionic character, since the positive charge is localized on the protonated pyrrolidine nitrogen atom of the nicotine amine while the negative charge is found in the vicinity of three chlorine atoms. The Zn-Cl distances range from 2.2334(11) to 2.2772(11) Å and the Zn-N bond length is 2.063(3) Å, which are comparable to those previously reported [22, 23]. The bond angles around the Zn atom range from 103.74 (10) to 114.20 (5)Å, values close to those expected for a regular tetrahedron, and agree with those found for other similar compounds [24]. As for the nicotine ligand, the pyridine and pyrrolidinium rings are nearly perpendicular to each other, the interplanar angle being 88.84° (Fig. 4), which corresponds to an intramolecular separation of N1 and N2 nitrogen atoms of 4.668Å. These geometric parameters agree with the data related to 34 structures containing nicotine skeleton cited in Cambridge Structural Database (CSD) [25], where the mutual disposition of pyrrolidinium and pyridine rings, measured by their interplanar angle, varies from 52 to 90° and the separation of the two nitrogen atoms is in the range 4.161-4.963Å.

In the crystal lattice, the $ZnNCl_3$ tetrahedra are interconnected by water molecules via O-H…Cl hydrogen bonds to form chains extending along the *c*-axis (Figs. 2, 3). The organic entities are

inserted between the chains interacting through C-H…Cl and N-H…Cl hydrogen bonds (Fig. 3, Table 2).

Refining the structure in the acentric space group $P2_12_12_1$ gives a value of -0.007(6) for the Flack parameter [26]. This value shows that the atomic arrangement corresponds to the correct absolute structure.

*Hirshfeld surface*

Organic small molecule crystal packings are often dominated by the hydrogen bonding patterns. However, a crystal structure is determined by a combination of many forces, and hence all of the intermolecular interaction of a structure should be taken into account. Visualization and exploration of intermolecular close contacts of a structure is invaluable, and this can be achieved using the Hirshfeld surface. A large range of properties can be visualized on the Hirshfeld surface with program CrystalExplorer [20] including the distance of atoms external, $d_e$, and internal, $d_i$, to the surface. The intermolecular distance information on the surface can be condensed into a two-dimensional histogram of $d_e$ and $d_i$, which is a unique identifier for molecules in a crystal structure, called a fingerprint plot [27, 28].

Instead of plotting $d_e$ and $d_i$ on the Hirshfeld surface, contact distances are normalized in CrystalExplorer using the van der Waals radius of the appropriate internal and external atom of the surface:

$$d_{norm}= (d_i - r_i^{vdw})/ r_i^{vdw}+ (d_e - r_e^{vdw})/ r_e^{vdw}$$

The program is the basis for rigorous quantitative analysis of molecular properties for comparison with bulk measurement and for convenient comparison of molecules in different molecular environments. Analysis of intermolecular interactions using the Hirshfeld surface-based tools represents a major advance in enabling supramolecular chemists and crystal engineers to gain insight into crystal packing behavior. Then, the surface colored according to

$d_{norm}$ values shows where the short intermolecular interactions occur; on the Cl1 chlorine atom for instance in Fig. 5. The Hirshfeld surface was computed for $C_{10}H_{15}Cl_3N_2Zn{\cdot}H_2O$ and therefore the analysis does not take into account the contacts between the water molecule and the organometallic part occurring within the asymmetric unit The fingerprint plot of the intermolecular contacts for the title compound are shown in Fig. 6.

Globally, H…Cl and H…H intermolecular interactions are the most abundant in the crystal packing (44.5% and 39.3 % respectively). There are indeed five H…Cl hydrogen bonds in the crystal structure (Table 3, Fig. 6a) and this type of interaction appears to have enriched occurrences (Table 4). Figure 7 also highlights visually that chlorine and hydrogen are often mutual partners in the crystal contacts.

The chlorine atoms present in the $ZnCl_3$ anion are much more electronegative than the chlorine atoms present in organic molecules which are less charged and have a more hydrophobic behavior. Three H-bonds out of six involving the chlorine atoms are with polar hydrogen atoms. Organic chlorine would conversely favor interactions with less polar H-C type hydrogen atoms [30]. The H…H contacts are the second most frequent interactions due to the abundance of hydrogen on the molecular surface (Fig. 6b), but they are slightly under-represented with an enrichment ratio of 0.89 (Table 4).

The H…O hydrogen bonds account for 6.7% of the total Hirshfeld surface (Fig. 6c) and are over-represented (enrichment $E_{HO}$=1.47). The C…H interactions (Fig. 6d) constitute only 2.5% of the contacts and appear significantly under-represented: if all contact types were equiprobable they would represent as much as 6.3% of the interaction surface.

The contact analysis for this compound suggests that the enriched H…Cl and H…O hydrogen bonds are the driving force in molecular arrangement and crystal packing formation. Cl…Cl contacts, which represent only 0.4% on the Hirshfeld surface, are extremely impoverished in

the crystal (enrichment $E_{ClCl}$=0.08), as the chlorine atoms bound to zinc and the $ZnCl_3$ group as whole are electronegative, therefore the Cl…Cl contacts are electrostatically repulsive.

The electrostatic potential was determined by Avogadro 1.0.0 software package [21]. Fig. 8 shows that a positive electrostatic potential is localized over the organic cation while the $ZnCl_3$ part is more electronegative. According to these results, we can say that there is a global electrostatic attraction between the $ZnCl_3$ anion and the organic cation which adds up to the favorable H…Cl hydrogen bonding.

*Quantum mechanical study*

Quantum chemical calculation was performed from the crystal data with DFT method at the 6-311++G(d,p) basis set, using Gaussian 03 program [32]. The energies of HOMO and LUMO are −5.210 and -3.125 eV, respectively. The large HOMO-LUMO gap is 2.085 eV, implies high kinetic stability and low chemical reactivity, because it is energetically unfavorable to add electron to a high-lying LUMO, to extract electrons from low-lying HOMO [33].

In order to study their electronic structure, frontier molecular compositions for various types of atoms in the frontier molecular orbitals were expressed as the atomic orbital coefficient square sum in the type of atomic orbitals and corrected by normalizing the specific molecule orbital [34]. The stereographs of frontier molecular orbital of the compound are shown in Fig. 9.

Orbital contribution investigation indicates: the composition of HOMO comes mainly from orbitals of $ZnCl_3$ and water molecule. In contrast, the components of LUMO come mainly from the pyridine ring. These results show that the electrons are mainly delocalized in the $ZnCl_3$ anion and in the water molecule.

*NMR results*

The $^{13}$CCP–MAS NMR spectrum of the title compound (Fig. 10) is in good agreement with the X-ray structure. Indeed, it exhibits ten well-defined resonances corresponding to the ten crystallographically independent carbon atoms, in agreement with only one organic molecule in the asymmetric part of the unit cell.

$^{15}$N CP–MAS NMR spectrum of the title compound (Fig. 11) is also in good agreement with the X-ray structure. Indeed, it exhibits two well-defined resonances at -332.7 and -139.2 ppm corresponding to the two crystallographically independent nitrogen atoms, in agreement with only one organic molecule in the asymmetric part of the unit cell.

Theoretical calculations were undertaken in order to assign the NMR resonances to the different crystallographically inequivalent atoms of the unit cell. The atoms are labeled as depicted in Scheme I:

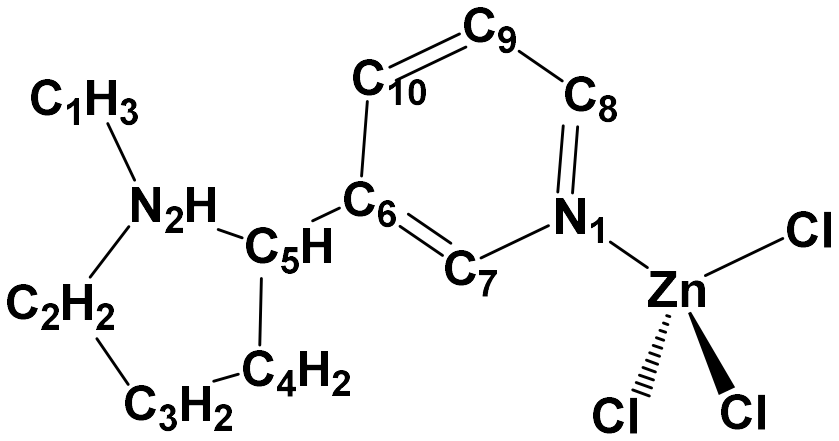


Scheme I. Atom labels.

Three different calculations were made on the organisation and, in all cases, the theoretical chemical shifts were subtracted from those of the reference (tetramethylsilane for carbon with $\delta_{exp}$ = 0 ppm and glycine for nitrogen with $\delta_{exp}$ = -347.2 ppm) calculated at the same level of theory:

(1) Calculation of the NMR chemical shifts (with the GIAO method) by using the positions of atoms obtained by X-ray diffraction;

(2) Optimization of the positions of the protons in the above molecule and calculation of the NMR chemical shifts in this semi-optimized geometry. Indeed X-ray diffraction leads always to underestimate X-H bond lengths, due to the fact that it is sensitive to the electronic cloud and does not see the nuclei;

(3) Full optimization of all atoms and calculation of NMR chemical shifts. This calculation, compared to the above ones can give indications on the steric hindrance around the organisation and on the positions where it is the strongest.

Since there are two possible positions for the C8 atom methylene group, two calculations were made for each of the positions. The results are listed on Table 4 and Fig. 12. Clearly, there is a very good agreement between the experimental and the theoretical values calculated after optimization of the position of the protons, allowing unambiguously the attribution of the different NMR signals. The discrepancies between the experimental and calculated chemical shifts are due to the fact that the experimental spectrum has been recorded in the solid state, while the theoretical chemical shifts correspond to the isolated molecule of the compound. It is worthy to note that the number of NMR signals corresponds to a single organic molecule, which is probably due to a moderate effect between the two positions found by X-rays. That is why the attribution was made, each time, taking the average of the two extreme positions.

*IR spectroscopy*

FTIR spectroscopy was used to identify the functional groups present in the crystal. The infrared absorption spectrum of the title compound is shown in Fig. 13. A detailed assignment of all bands observed in the infrared spectrum of the cation in the title compound is based on the comparison with other similar materials [35]. In the domain of high frequencies, the bands between 3429 and 2617 $cm^{-1}$ are due to the stretching vibration frequencies of the O-H, N-H

and C-H bonds interconnected by a system of hydrogen bonds in the crystal. The band at 1639 $cm^{-1}$ is assigned to the N-H bending mode. The bands between 1592 and 1500 $cm^{-1}$ are attributed to the C=C and C=N stretching modes of the pyridine [36]. The absorption band located at 1260 $cm^{-1}$ corresponds to the $\delta(CH_3)$ modes. The band at 1103 $cm^{-1}$ can be attributed to the $\gamma(CH_3)$ mode. The band observed at 1071 and 1015 $cm^{-1}$ be assigned to the δ (CH) and γ ($CH_3$) modes. The band observed at 950 $cm^{-1}$ can be assigned to the γ(CH) mode. The remaining bands at 793 and 700 $cm^{-1}$ are assigned to γ(CH) and δ(CH) modes. The bands observed at 827, 548, 462 and 496 $cm^{-1}$, are related to the skeletal [35].

## Conclusion

A new non-centrosymmetric(S)-nicotiniumtrichloridozincate monohydrate complex has been prepared at room temperature and characterized by physicochemical methods. On the structural level, it can be described as built up by chains of $ZnNCl_3$ tetrahedra and water molecules, interconnected via O-H…Cl hydrogen bonds. Between theses chains, the organic entities are inserted through C-H…Cl and N-H…Cl hydrogen bonds. The Hirshfeld surface analysis with fingerprint plots and electrostatic potential map reveals the percentage of intermolecular contacts and distribution of electrostatic potential of the title compound. The number of $^{13}C$ and $^{15}N$ CP–MAS NMR lines is in full agreement with the crystallographic data. DFT calculations allow the attribution of the experimental NMR lines. The vibrational absorption bands were identified by infrared spectroscopy.

## Supplementary data

Crystallographic data for the structural analysis have been deposited at the Cambridge Crystallographic Data Centre, CCDC No1061474. These data can be obtained free of charge via http://www.ccdc.cam.ac.uk/conts/retrieving.html, or from the CCDC, 12 Union Road, Cambridge, CB2 1EZ, UK: fax: (+44) 01223-336-033; e-mail: deposit@ccdc.cam.ac.

**References**


[1] K.C. Gupta, A. Kumar Sutar, Coord. Chem. Rev. 252, (2008) 1420-1450.

[2] Y.N. Belokon, W. Clegg, R.W. Harrington, M. North, C. Young, Inorg. Chem. 47 (2008) 3801-3814.

[3] N. Farrell, Transition Metal Complexes as Drugs and Chemotherapeutic Agents, in *Catalysis by Metal Complexes*, 11, (1989).

[4] V. Balzani, A. Juris, M. Venturi, S. Campagna, S. Serroni, Chem. Rev. 96, (1996) 759-833

[5] H. Sakurai, Y. Kojima, Y. Yoshikawa, K. Kawabe, H. Yasui, Coord. Chem. Rev. 226 (2002) 187–198.

[6] S. -F. Lu , D.-M. Du , J. Xu, S.-W. Zhang, J. Am. Chem. Soc., 128 (2006), 7418–7419.

[7] C.-Y. Sung **,** C.-Y. Li **,** J.-K. Su **,** T.-Y. Chen **,** C.-H. Lin, B.-T.Ko, DaltonTrans., 41, (2012), 953-961.

[8] P.S. Subramanian, D. Srinivas, Polyhedron, 15 (1996) 985-989.

[9] B.H. Ye, X. M. Chem, G.Q. Xue, L.N. Ji, J. Chem. Soc. Dalton Trans.17 (1998) 2827-2832.

[10] K. Keller, P.J. Whitehouse, A.M. Maatino-Barrow, K. Marcus, D.L. Price, BrainRes. 436 (1987) 62–68.

[11] P.A. Newhouse, Y. Sunderland, P.N. Tariot, C.L. Blumhardt, H. Weingartner, A. Mellow, Psychopharmacology 95 (1988) 171–175.

[12] K. H. Kim, N. Lin, D. J. Anderson, Bioorg. Med. Chem. 4 (1996) 2211–2217.

[13] M. W. Holladay, M. J. Dart, J. K. Lynch, J. Med. Chem. 40 (1997) 4169–4190.

[14] R. H. Blessing, ActaCryst. A51 (1995) 33-38.

[15] A. Altomare, M. C. Burla, M. Camalli, G. Cascarano, C. Giacovazzo, A. Guagliardi, A. G. Moliterni, G. Polidori, R. Spagna, J. Appl. Cryst. 32 (1999) 115-119.

[16] G. M. Sheldrick, SHELXL, Version 2014/3, Program for Crystal Structure Refinement, University of Göttingen, 2014.

[17] L. J. Farrugia, Appl. Cryst. 32 (1999) 837-838.

[18] K. Brandenburg , DIAMOND version 2.0, 1998.

[19] C. F. Macrae, P. R.Edgington, P. McCabe, E. Pidcock, G. P. Shields, R. Taylor, M. Towler, J. van de Streek, J. Appl. Cryst.39 (2006) 453-457.

[20] J. J. McKinnon, M. A. Spackman, A. S. Mitchell, Acta Cryst B-Structural Science 2004, 60, 627-668.

[21] M. D. Hanwell, D. E. Curtis, D. C. Lonie,T. Vandermeersch, E. Zurek, G. R, Hutchison,"Avogadro: An advanced semantic chemical editor, visualization, and analysis platform".J. Cheminform. 4 (1) 2012.

[22] X. -F. Chen, S.-H. Liu, X.-H. Zhu, J.J.Vittal, E. -K. Tan, X.-Z.You, ActaCryst.C56 (2000) 42-43.

[23] L.R. Gahan, T.W. Hambley, A.M. Sargeson, M.R. Snow, Inorg. Chem. 21 (1982) 2699-2706.

[24] W.-T. Chen, D.-S. Liu, S.-M.Ying, H.-L. Chen, Y.-P. Xu, Inorg. Chem. Commun.11 (2008) 1212-1214.

[25] F. H. Allen, ActaCryst. B58 (2002) 380-388.

[26] S.Parsons,H. D. Flack,T.Wagner,ActaCryst. B69 (2013) 249 - 259.

[27] M. A. Spackman and P. G. Byrom, Chemical Physics Letters 1997, 267, 215-220.

[28] M. A. Spackman and J. J. McKinnon, Crystengcomm 2002, 378-392.

[29] B. Guillot, E. Enrique, L. Huder, C. Jelsch, Acta Cryst. (2014). A70, C279.

[30] C.Jelsch, S. Soudani, C. Ben Nasr,IUCr J. (2015) 2, 327-340.

[31] C. Jelsch, K. Ejsmont, L. Huder, IUCrJ 1 (2014) 119-128.

[32] M. J. Frisch, G. W. Trucks, H. B. Schlegel, G. E. Scuseria, M. A.Robb, J. R.Cheeseman, J. A. Jr. Montgomery, T. Vreven, K. N. Kudin, J. C.Burant, J. M.Millam, S. S.Iyengar, J.Tomasi, V. Barone, B.Mennucci, M.Cossi, G.Scalmani, N.Rega, G. A.Petersson, H.Nakatsuji, M.Hada,M.Ehara, K. Toyota, R. Fukuda, J. Hasegawa, M. Ishida, T. Nakajima, Y. Honda, O.Kitao, H.Nakai, M. Klene, X. Li, J. E. Knox,H. P.Hratchian,J. B. Cross,C.Adamo,J. Jaramillo,R.Gomperts,R. E.Stratmann,O.Yazyev,A. J.Austin,R. Cammi,C. Pomelli, J. W. Ochterski,P. Y.Ayala,K.Morokuma,G. A.Voth,P. Salvador,J. J.Dannenberg,V. G. Zakrzewski,S.Dapprich, A. D. Daniels,M. C. Strain,O.Farkas,D. K.Malick, A. D.Rabuck, K.Raghavachari,J. B. Foresman,J. V.Ortiz,Q. Cui,A. G.Baboul, S. Clifford, J. Cioslowski, B. B. Stefanov,G. Liu,A.Liashenko,P.Piskorz,I.Komaromi,R. L.Martin,D. J.Fox,T. Keith,M. A. Al-Laham,C. Y.Peng,A. Nanayakkara,M.Challacombe,P. M. W. Gill,B. Johnson,W. Chen,M. W.Wong,C. Gonzalez,Pople, J. A. Gaussian 03, Revision B.01, Gaussian, Inc., Pittsburgh PA 2003.

[33] Z. L.Wang,L. H.Wei, L. Y.Jin, J. P. Wang, Chin. J. Struct. Chem. 2007, 26, 1423−1428.

[34] J.Zhang, B. Q. Yang, H. Y.Zhu,T.Li,Z. Y. Wen, Chin. J. Chem. 2006, 24, 637−641.

[35] B. Jasiewicz, K. Malczewska-Jaskóła, I. Kowalczyk, B. Warżajtis, U. Rychlewska, Spectrochim. Acta Mol. Biomol. Spectrosc.128 (2014) 773–780.

[36] E. P. Parry, J. Catal. 2 (1963) 371-379.

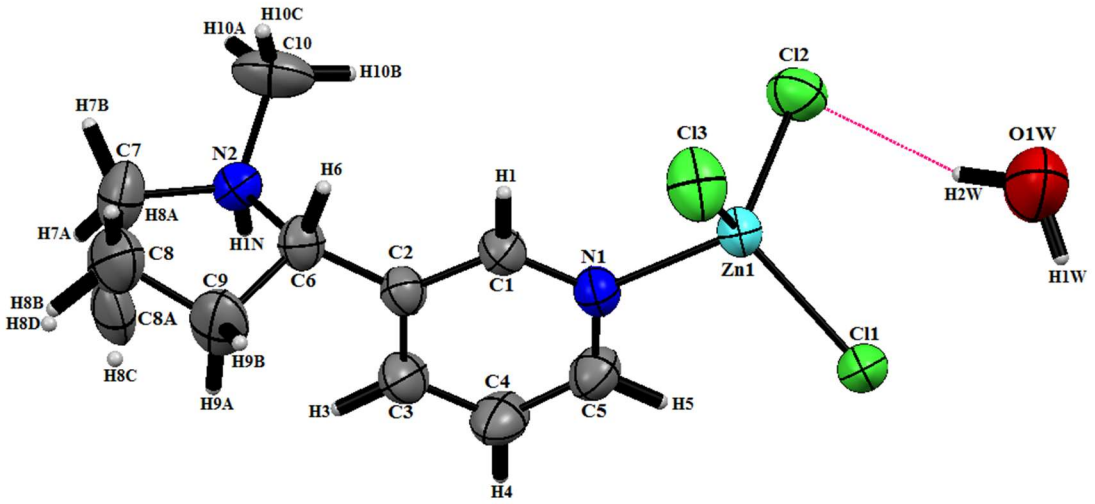


**Figure 1** A view of the asymmetric unit in the crystal structure of the title compound showing the atom-numbering scheme and thermal displacement ellipsoids drawn at the 50% probability level. The dotted lines indicate hydrogen bonds.

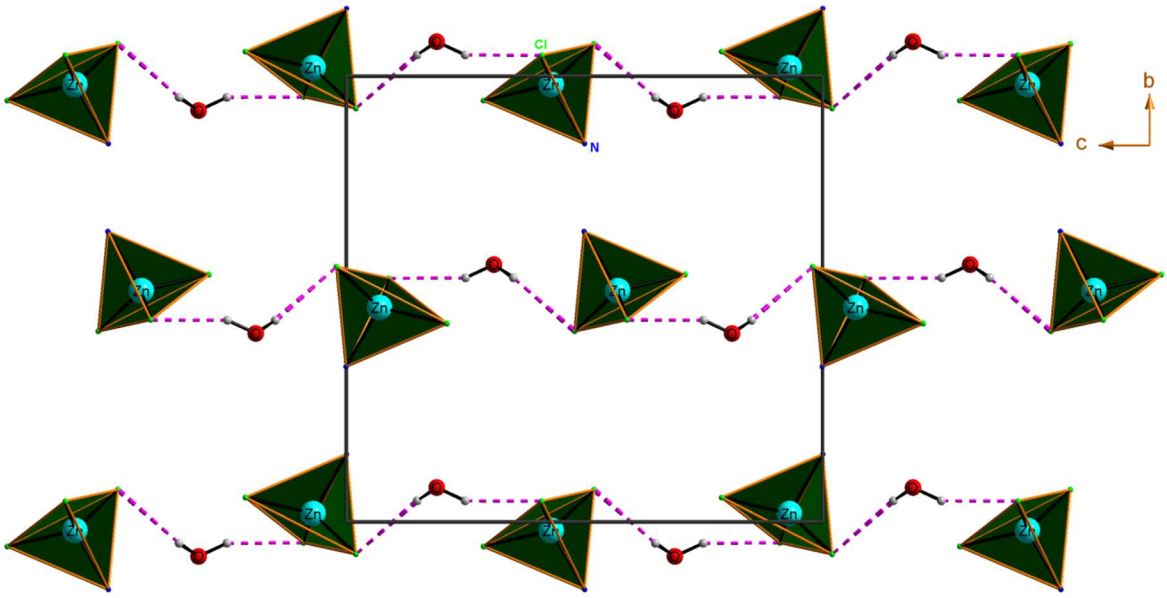


**Figure 2**

Projection along the *a*-axis showing the chains of water and of the inorganic moiety $ZnCl_3$ in the crystal of the title compound. Hydrogen bonds are denoted by dotted lines.

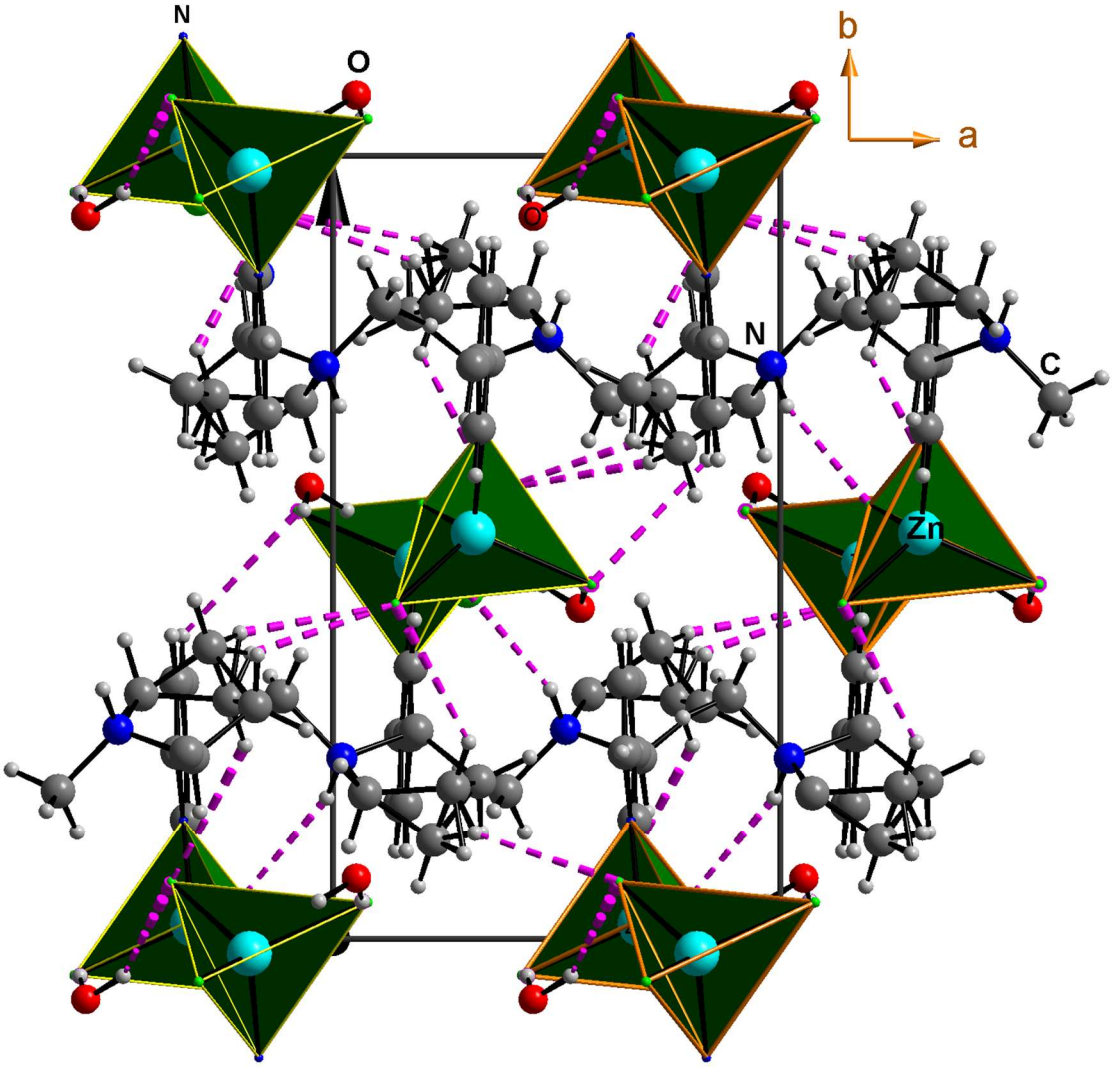


**Figure 3** Projection along the *c*-axis of the crystal packing of the title compound. The purple dotted lines indicate hydrogen bonds.

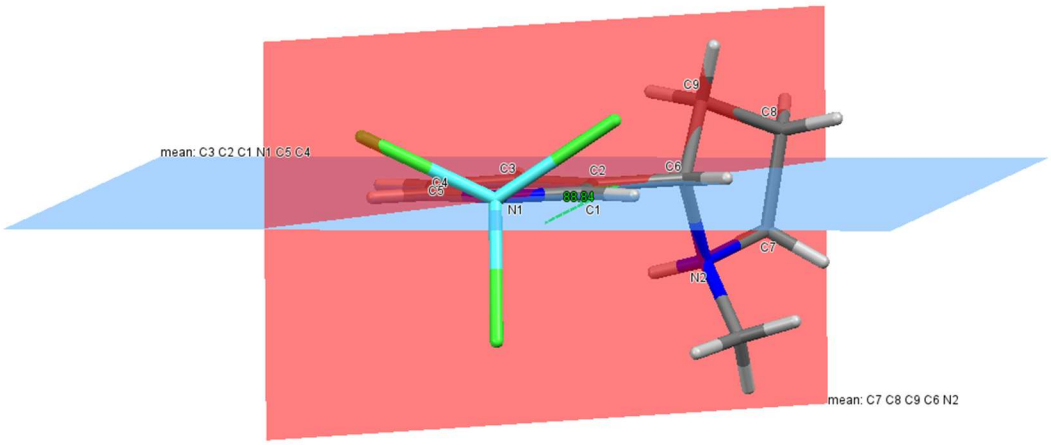


**Figure 4** Mutual disposition of pyridine and pyrrolidinium rings in the crystal of the title compound.

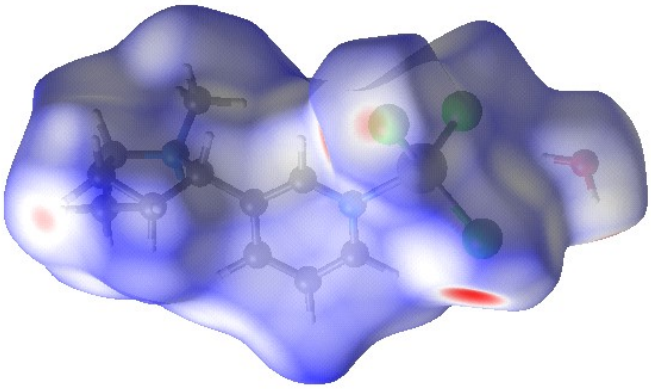

**Figure 5** Hirshfeld surface around the asymmetric unit colored according to $d_{norm}$.

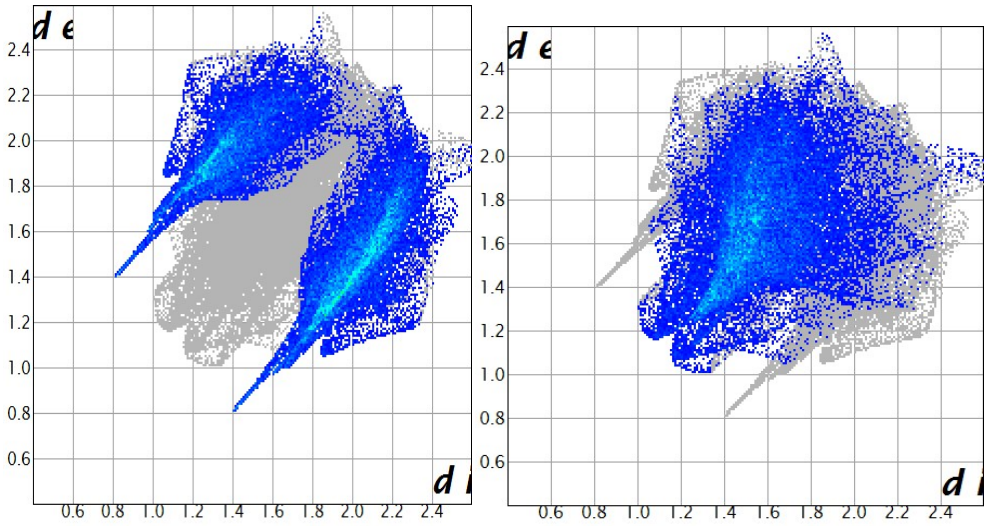


**(a) H…Cl/Cl…H : 44.5%** **( b) H…H : 39.3%**

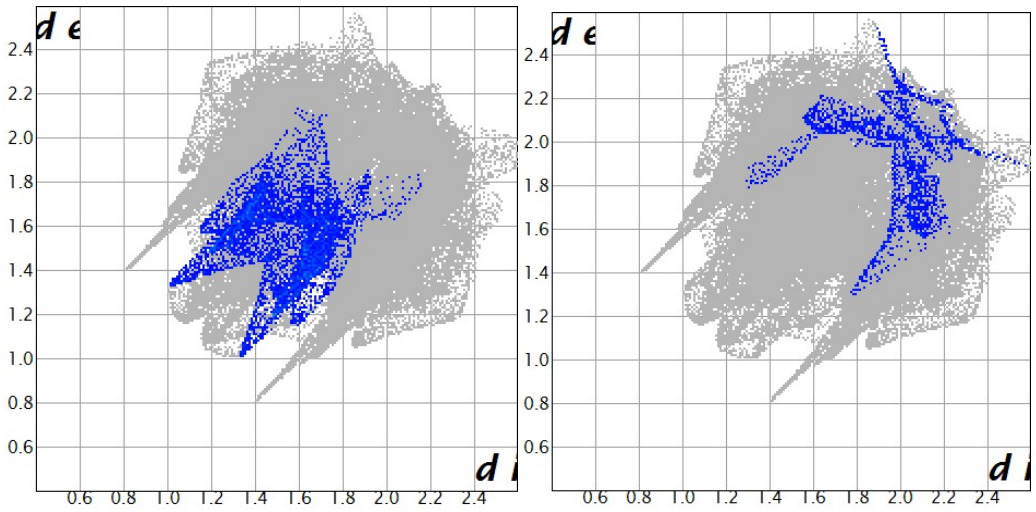


**(c) H…O/O…H: 6.7%** **(d)C…H /H…C: 2.5%**

**Figure 6**. Fingerprint plots of the major contacts:

(a) H···Cl, (b) H··H, (c) H···O and (d) C…H.

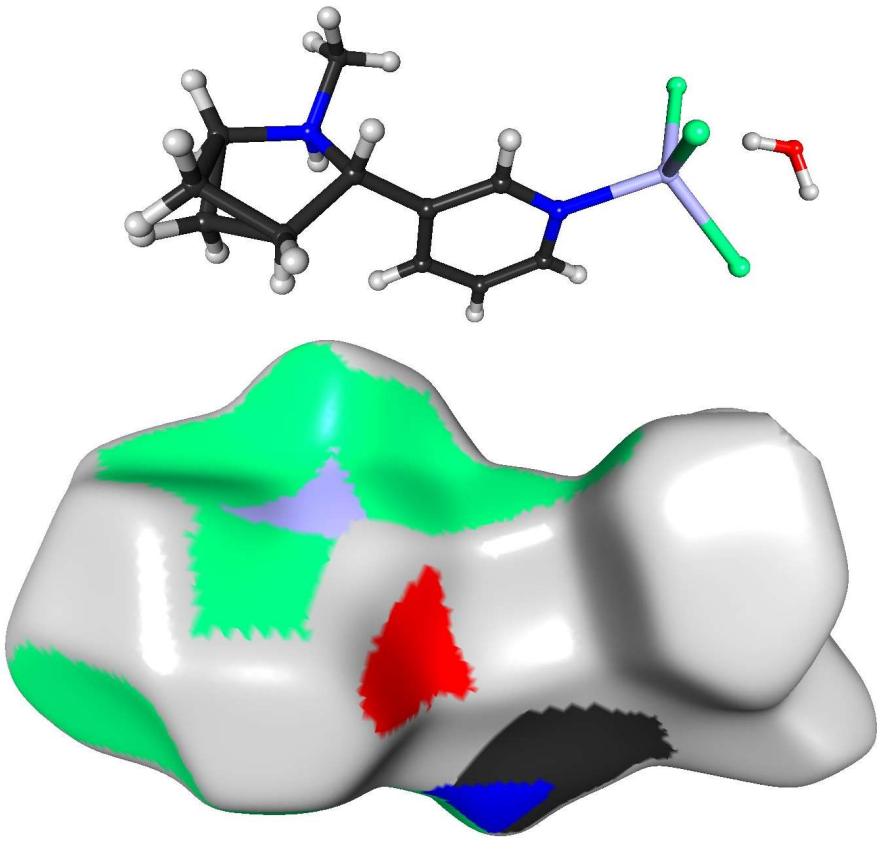

**Figure.7** Hirshfeld surface around the $C_{10}H_{15}Cl_3N_2Zn$ moiety colored according to the chemical type of the closest interacting atom in the crystal surrounding. The orientation of the molecule (with same atom colors) is shown on the top. The figure was generated with MoProViewer [29]

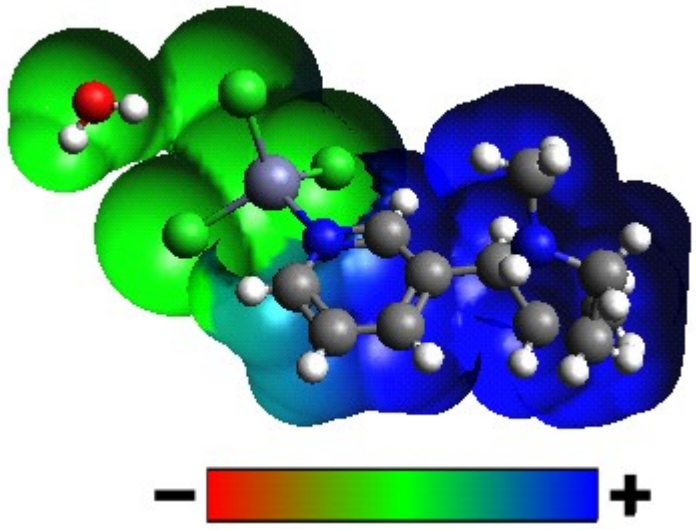


**Figure.8** Electrostatic potential (red: negative potential, blue: positive potential).

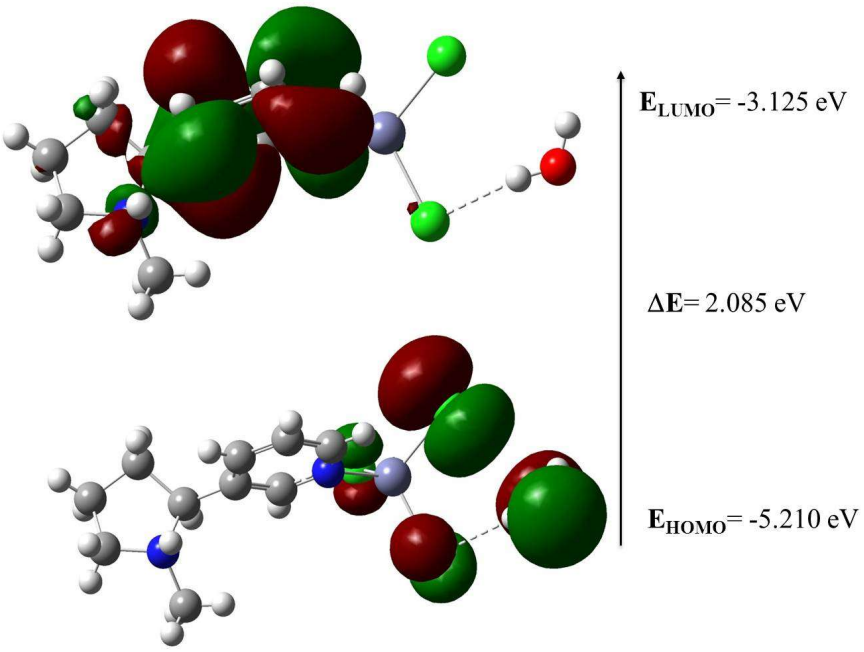


**Figure 9** Frontier molecular orbitals (HOMO and LUMO).

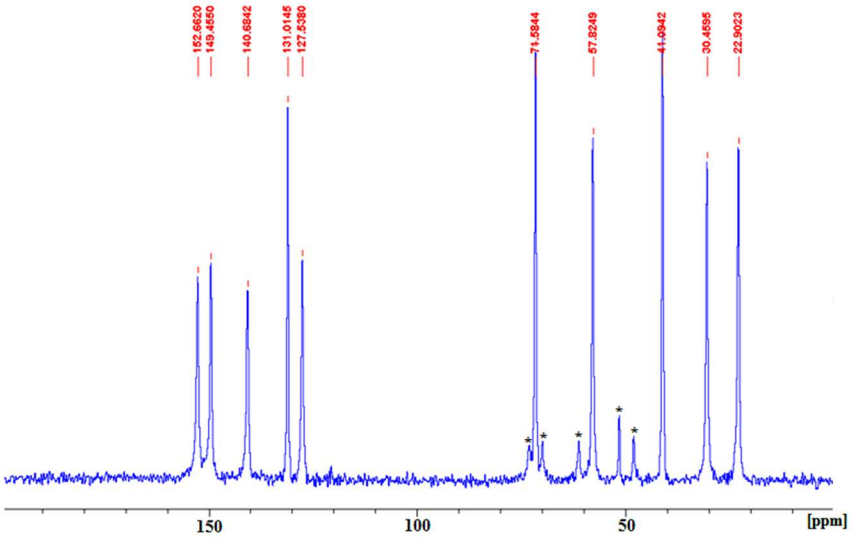


**Figure. 10** $^{13}C$ CP-MAS NMR spectrum of $C_{10}H_{15}Cl_3N_2Zn \cdot H_2O$.

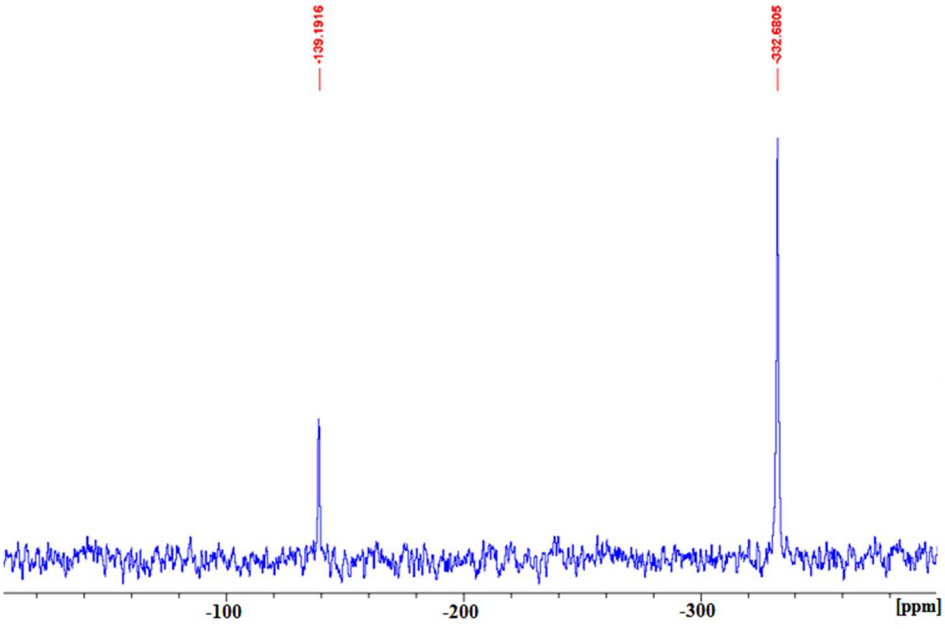


**Figure. 11** $^{15}N$ CP-MAS NMR spectrum of$C_{10}H_{15}Cl_3N_2Zn \cdot H_2O$.

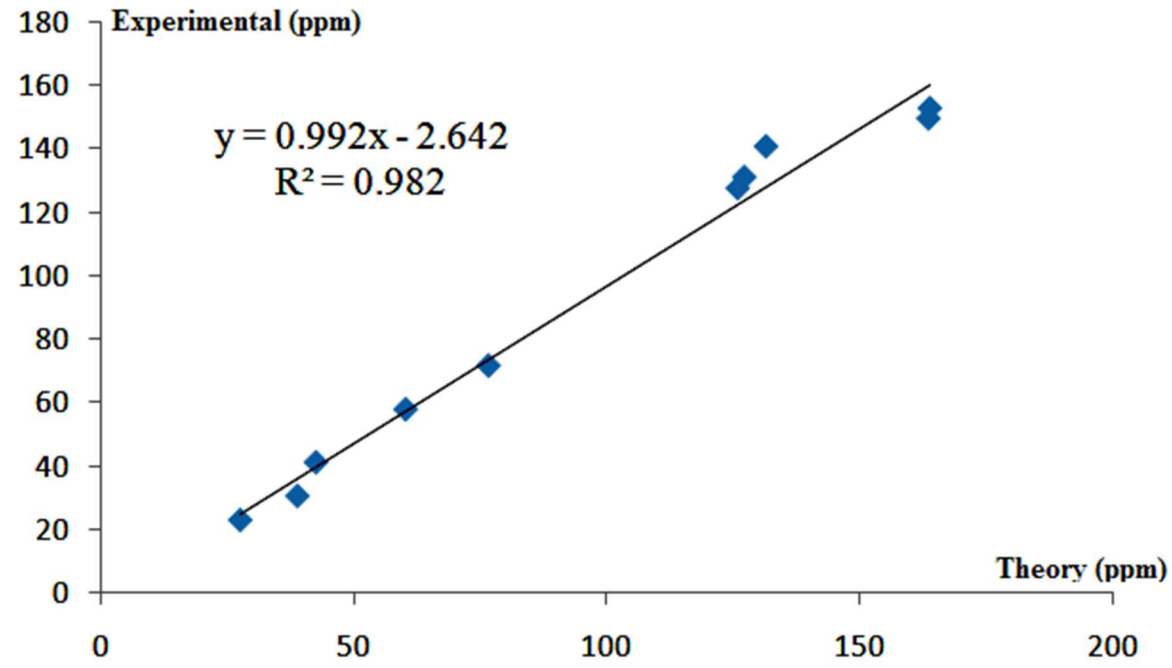


**Figure.12** Comparison between experimental and calculated IR frequencies of $C_{10}H_{15}Cl_3N_2Zn \cdot H_2O$

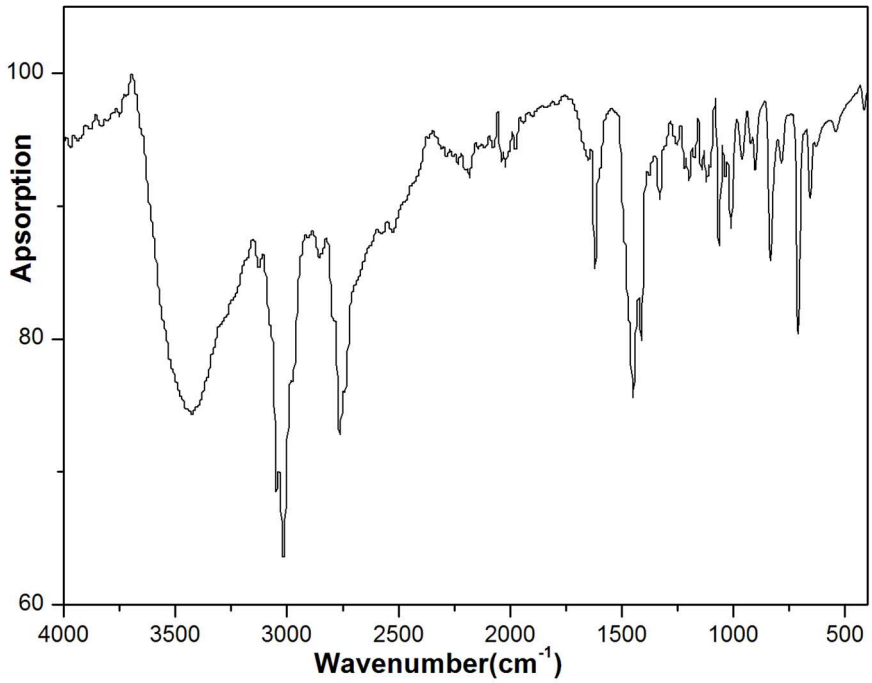


**Figure.13** Infrared absorption spectrum of$C_{10}H_{15}Cl_3N_2Zn \cdot H_2O$.

**Table 1**. Experimental details of $C_{10}H_{15}Cl_3N_2Zn·H_2O$ crystal.

| | |
|---|---|
| **Crystal data** | |
| Chemical formula | $C_{10}H_{15}Cl_3N_2Zn·H_2O$ |
| $M_r$ | 352.97 |
| Crystal system, space group | orthorhombic , $P2_12_12_1$ |
| Temperature (K) | 295 |
| $a$, $b$, $c$ (Å) | 7.6953 (2),13.4714 (4), 14.4295 (5) |
| $V$ (Å$^3$) | 1495.86 (8) |
| $Z$ | 4 |
| Radiation type | Mo $K\alpha$ |
| μ (mm$^{-1}$) | 2.16 mm$^{-1}$ |
| Crystal size (mm) | 0.55 × 0.29 × 0.15 |
| measured, independent and observed [$I > 2\sigma(I)$] reflections | 11876, 3566, 3249 |
| $R_{int}$ | 0.042 |
| **Refinement** | |
| $R[F^2 > 2\sigma(F^2)]$, $wR(F^2)$, $S$ | 0.035, 0.103, 1.16 |
| No. of reflections used | 3566 |
| No. of parameters | 171 |
| No. of restraints | 0 |
| Absolute structure parameter | -0.007(6) |

**Table 2.** Selected bond distances and angles *(*Å, º*)*

| | | | |
|---|---|---|---|
| Zn1—N1 | 2.063 (3) | C1—C2 | 1.382 (5) |
| Zn1—Cl2 | 2.2334 (12) | C2—C3 | 1.395 (6) |
| Zn1—Cl3 | 2.2348 (13) | C4—C5 | 1.379 (6) |
| Zn1—Cl1 | 2.2772 (11) | C6—C9 | 1.536 (6) |
| N1—C5 | 1.340 (5) | C8A—C7 | 1.473 (13) |
| N1—C1 | 1.344 (5) | C8—C9 | 1.494 (13) |
| N2—C7 | 1.497 (6) | C8—C7 | 1.525 (15) |
| N2—C10 | 1.485 (6) | C8A—C9 | 1.589 (11) |
| N2—C6 | 1.516 (5) | C5—N1—Zn1 | 122.1 (3) |
| N1—ZN1—Cl2 | 109.51 (10) | C1—N1—Zn1 | 119.7 (3) |
| N1—Zn1—Cl3 | 103.74 (10) | C10—N2—C7 | 114.2 (4) |
| Cl2—Zn1—Cl3 | 113.77 (5) | C10—N2—C6 | 113.4 (4) |
| N1—Zn1—Cl1 | 106.71 (10) | C7—N2—C6 | 106.4 (3) |
| Cl2—Zn1—Cl1 | 108.52 (5) | C5—N1—C1 | 118.2 (3) |
| Cl3—Zn1—Cl1 | 114.20 (5) | C9—C8—C7 | 103.2 (8) |
| C1—C2—C3 | 117.0 (4) | C7—C8A—C9 | 101.1 (7) |
| C1—C2—C6 | 120.2 (3) | C2—C6—C9 | 116.6 (4) |
| C4—C3—C2 | 120.2 (4) | N2—C6—C9 | 103.1 (3) |
| C3—C2—C6 | 122.8 (3) | C8—C9—C6 | 104.0 (6) |
| N1—C1—C2 | 123.4 (4) | C8A—C7—N2 | 102.4 (5) |
| C3—C4—C5 | 118.6 (4) | N2—C7—C8 | 107.7 (6) |
| N1—C5—C4 | 122.5 (4) | C6—C9—C8A | 105.7 (5) |
| C2—C6—N2 | 111.2 (3) | | |

**Table 3**. Hydrogen-bond geometry (Å, °)

| *D*—H···*A* | *D*—H | H···A | *D*···*A* | *D*—H···*A* |
|---|---|---|---|---|
| O1W—H2W···CL2 | 0.954 | 2.322 | 3.212 (6) | 155.15 |
| C6—H6···CL1$^{i}$ | 0.98 | 2.96 | 3.925 (4) | 169.88 |
| C8—H8A···CL3$^{i}$ | 0.97 | 2.99 | 3.777 | 139 |
| C8—H8B···CL3$^{ii}$ | 0.97 | 2.75 | 3.513 | 137 |
| C8A—H8D···CL3$^{ii}$ | 0.97 | 2.87 | 3.702 | 144 |
| N2—H1N···CL1$^{iii}$ | 0.88 (6) | 2.33 (5) | 3.161 (4) | 156.31 |
| O1W—H1W···CL3$^{iv}$ | 0.961 | 2.597 | 3.497 (6) | 155.82 |

Symmetry codes: (i) −x+3/2, −y+2, z−½; (ii) −x+1, y− ½ , −z+1/2; (iii) x+½, −y+3/2, −z+1; (iv) −x+3/2, −y+2, z+½.

**Table 4**. Chemical proportions on the Hirshfeld surface and major interaction types.

The enrichment ratio of contacts [31], highlights if interactions are over or under-represented in the crystal as compared to equiprobable contacts occurring with the same chemical content on the surface.

| Surface | H | C | N | O | Cl |
|---|---|---|---|---|---|
| Content (%) | 66.5 | 4.8 | 1.5 | 3.4 | 22.8 |
| Major contacts | H…Cl | H…H | H…O | C…H | |
| Proportion (%) | 30.3 | 39.3 | 4.5 | 2.5 | |
| Enrichment $E_{xy}$ | 1.47 | 0.89 | 1.48 | 0.4 | |

**Table 5**. Comparison of calculated and experimental chemical shift values of the carbon and nitrogen atoms in $C_{10}H_{15}Cl_3N_2Zn \cdot H_2O$.

| Atoms | X-Rays | | Optimisation of protons | | | Optimisation of all atoms | Experimental |
|---|---|---|---|---|---|---|---|
| | Position 1 | Position 2 | Position 1 | Position 2 | Average | | |
| C1 | 21.2 | 20.3 | 43.5 | 41.7 | 42.6 | 47.8 | 41.1 |
| C2 | 43.2 | 29.2 | 59.5 | 61.2 | 60.3 | 61.0 | 57.8 |
| C3 | 9.0 | 28.3 | 25.4 | 29.8 | 27.6 | 31.3 | 22.9 |
| C4 | 20.8 | 13.3 | 37.5 | 40.3 | 38.9 | 31.0 | 30.5 |
| C5 | 71.9 | 69.0 | 81.0 | 73.4 | 76.7 | 78.8 | 71.6 |
| C6 | 121.6 | 127.6 | 126.5 | 128.1 | 127.3 | 134.4 | 131.0 |
| C7 | 160.3 | 155.9 | 166.2 | 161.8 | 164.0 | 165.8 | 152.7 |
| C8 | 155.1 | 160.0 | 161.7 | 165.6 | 163.7 | 163.6 | 149.5 |
| C9 | 126.4 | 121.7 | 125.0 | 127.0 | 126.0 | 131.5 | 127.5 |
| C10 | 127.3 | 126.5 | 131.4 | 131.8 | 131.6 | 138.7 | 140.7 |
| N1 | -28.6 | -28.8 | -27.8 | -28.3 | -28 | -33.9 | -139 |
| N2 | -302.7 | -290.1 | -273.8 | -257.2 | -265.5 | -266.9 | -332 |